Separation and Purification Technology 361 (2025) 131207

Contents lists available at ScienceDirect

Separation and Purification Technology

journal homepage: www.elsevier.com/locate/seppur

Capturing and converting CO_2 using amino acids as various commercially valuable nano-carbonates

Qingyang Li [a,b], Yong Qian [c], Malcolm Xing [d], Bingyun Li [a,*]

[a] Biomaterials, Bioengineering & Nanotechnology Laboratory, Department of Orthopaedics, West Virginia University, Morgantown, WV 26506, United States
[b] Department of Chemical and Biomedical Engineering, West Virginia University, Morgantown, WV 26506, United States
[c] Pathology and Physiology Research Branch, Health Effects Laboratory Division, National Institute for Occupational Safety and Health, Morgantown, WV 26505, United States
[d] Department of Mechanical Engineering, University of Manitoba, Winnipeg, MB R3T 5V6, Canada

ARTICLE INFO

Keywords:
Carbon dioxide
Amino acid
Nano-carbonate
Nanoparticle

ABSTRACT

Carbon dioxide (CO_2) is the most significant greenhouse gas and one of the strategies to reduce CO_2 emission is to convert CO_2 into commercially valuable products. Currently, methods that can effectively capture and convert CO_2 into carbonate nanomaterials, which have unique applications in various fields, have rarely been reported, and there are no universal methods that can capture and convert CO_2 into different nano-carbonates. In this study, an innovative two-step strategy based on amino acids was developed to produce multiple different carbonate nanoparticles, including $CaCO_3$, $BaCO_3$, and Ag_2CO_3 nanoparticles with diameters of 70 nm, 50 nm, and 7 nm, respectively. Fundamentally important, the nuclear magnetic resonance data clearly demonstrated that it was the amino acids (e.g., glycine) that dictated the formation of carbonate nanoparticles. In the presence of amino acids, a competition in forming nanoparticles and microparticles was observed, and the formation of nanoparticles was proportional to the carbamate formed from CO_2 reacting with amino acids. In the absence of amino acids, carbonate microparticles (~ 2 μm) were formed.

1. Introduction

The emission of carbon dioxide (CO_2), the most significant greenhouse gas, impacts the global climate because CO_2 traps heat from the sun in the Earth's atmosphere. Yet human activities, such as burning fossil fuels, have been continuing to elevate the atmospheric CO_2 level, leading to multiple environmental crises, including severe weather events (hurricanes, droughts, heavy rains, and wildfires) and rising sea levels.

In response, the global community has been exploring various strategies, including carbon capture and storage (CCS) and carbon capture and utilization (CCU) that target mitigating and reducing CO_2 emissions. CCS entails capturing CO_2 emissions from major CO_2 sources like power plants and industrial processes followed by their sequestration in deep underground formations. CCU, on the other hand, seeks not only to capture but also to convert CO_2 into valuable products, thus potentially offsetting the costs associated with CO_2 management. Among various CCU strategies, converting CO_2 into stable minerals such as calcium carbonate ($CaCO_3$) is emerging as a promising avenue, largely because such a CO_2 conversion process is thermodynamically favored—the Gibbs free energy of carbonates is lower than that of CO_2, making the reaction energetically favorable [1–3]. Calcium ion (Ca^{2+}) and magnesium ion (Mg^{2+}) are among the most extensively studied materials for CO_2 mineralization due to their reactivity and availability. For example, Oeiyono *et al.* [4] used an MEA solvent to capture CO_2 and subsequently mineralized the captured CO_2 into $CaCO_3$ particles by introducing CaO into the CO_2-saturated MEA solution. Liu *et al.* [2] utilized CaO, MgO, and $CaSiO_3$ to mineralize CO_2 captured by amino acid salt or monoethanolamine (MEA) solvents, forming $CaCO_3$ or $MgCO_3$. Huang *et al.* [5] employed protonated amines (e.g., MEA, 3-amino-1-propanol, 2-amino-2-methyl-1-propanol, diethanolamine, and N,N-dimethylethanolamine) as reagents to extract Ca^{2+} from coal fly ash, which was then used to stabilize CO_2 captured by the amines into $CaCO_3$. To enhance the value of $CaCO_3$, Madhav *et al.* [6] utilized polymers (polydopamine, polyvinyl alcohol, polyethylene glycol) to modify the formation of $CaCO_3$ during CO_2 capture and mineralization using $CaCl_2$ and L-arginine as the solvent. These strategies are of great interest even though their mineralized products were typically large

* Corresponding author.
E-mail address: bili@hsc.wvu.edu (B. Li).

https://doi.org/10.1016/j.seppur.2024.131207
Received 2 October 2024; Received in revised form 18 December 2024; Accepted 18 December 2024
Available online 19 December 2024

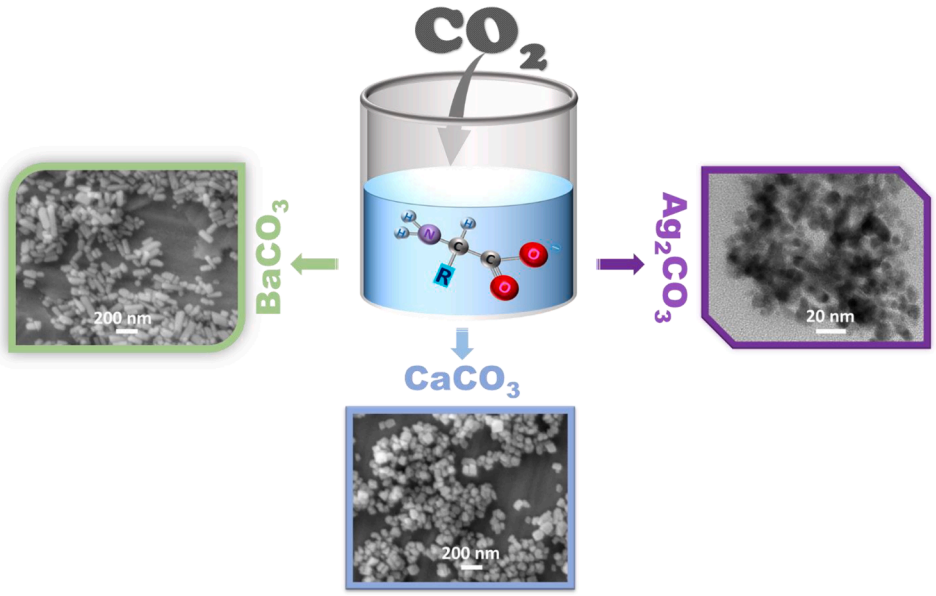

Fig. 1. Converting CO_2 into various nano-carbonates using an amino acid-driven process.

(micrometer or larger) along with wide size distributions.

Nanoparticles (particles with at least one dimension smaller than 100 nm) are well recognized for their dramatically altered properties from bulk materials [7–9]. Nanoparticles may be more valuable compared to their corresponding bulk size, and the nano-carbonate markets are quickly expanding. For instance, the global $CaCO_3$ nanomaterials market was valued at US$ 8.4 billion in 2022 and was anticipated to grow at a compound annual growth rate (CAGR) of approximately 9.7 % to exceed US$ 17 billion by 2030 [10,11]. Several methods, including precipitation, emulsion, polymerization, and mechano-chemical methods have been studied to produce $CaCO_3$ nanoparticles [12–16], and among them, few reports have shown the possibility of converting waste CO_2 into $CaCO_3$ nanoparticles. Unfortunately, these current methods require either additional external energy (e.g., heating the solvent to 90 °C [17]) or chelating agents (e.g., ethylenediaminetetraacetic acid [18] or L-Glutamic acid-N,N-diacetic acid tetrasodium salt [19]) that may create environmental concerns, and no studies so far have shown the production of carbonate nanoparticles at a large scale. No publications have been reported on converting CO_2 into other nano-carbonates (e.g., $BaCO_3$, Ag_2CO_3).

Here we report, for the first time, a straightforward, universal method that converts CO_2 into carbonate nanoparticles. Our method is environmentally friendly and does not require any additional energy input. Nano-carbonates of various metal ions (e.g., $CaCO_3$, $BaCO_3$, and Ag_2CO_3) with sizes of 70 nm, 50 nm, and 7 nm were successfully produced. Equally importantly, the role of amino acids in the synthesis of carbonate nanoparticles was clearly determined and no amino acids were consumed during the synthesis.

2. Experimental sections

2.1. Materials

L-glycine (Gly, ≥98 wt%), L-asparagine (Asn, ≥99 wt%), L-alanine (Ala, ≥98 wt%), L-Cysteine (Cys, ≥98.5 wt%), sodium hydroxide (NaOH, ≥98 wt%), potassium hydroxide (KOH, ≥98 wt%), calcium chloride ($CaCl_2$, ≥97 wt%), barium chloride ($BaCl_2$, ≥99 wt%), silver nitrate ($AgNO_3$, ≥99 wt%), deuterium oxide (D_2O, ≥99.9 wt%), and 1,4-dioxane (≥99.5 wt%) were purchased from MilliporeSigma (Burlington, MA). CO_2 (99.99 %) was purchased from Airgas (Radnor, PA). All chemicals were used as received.

2.2. CO_2 absorption and mineralization

Solvents for CO_2 absorption were prepared by dissolving a base and/or an amino acid at a certain molar ratio in 25 mL of water and mixing in 50-mL plastic centrifuge tubes. The method for CO_2 absorption experiments was detailed in our previous publications [20,21]. In brief, a 5-mL serological pipette was positioned at the base of each tube to serve as a CO_2 gas input. Mass flow controllers were used to regulate the flow rate at 100 standard cubic centimeters per minute (sccm). After bubbling, metal ion ($CaCl_2$, $BaCl_2$, $AgNO_3$) was added and the solvent was vortexed for 1 min to produce corresponding carbonates. Then precipitates were collected by centrifugation at 4,000 revolutions per minute (rpm) for 5 min and washed with deionized water. The centrifugation and washing were repeated four times to remove soluble chemicals from the solid products. The quantity of CO_2 absorbed was determined by measuring the mass of the solvent at various time intervals during the bubbling process. The weight of the precipitates was obtained using an analytical balance after vacuum drying the washed samples for 72 h. In addition, the pH of the solvents was monitored with an Apera MP511 Benchtop pH Meter. Triplicate samples were run for each experiment. The CO_2 loading and precipitates' weight were quantified by calculating the ratios of captured CO_2 (mol) to OH^- (mol) and carbonate (mol) to OH^- (mol), respectively.

2.3. Characterization

2.3.1. ^{13}C nuclear magnetic resonance (^{13}C NMR)

The ^{13}C NMR spectra, aimed at identifying carbon species, were obtained using a 400 MHz Agilent NMR instrument. 500 μL solvent sample, 200 μL D_2O (used as lock), and 15 μL 1,4 dioxane (used as a reference) were added in a 1-mL centrifuge tube, mixed thoroughly, and transferred into an NMR tube (S-5–600-7). ^{13}C NMR experiments were conducted with a delay time of 1 s along with 256 scans. To investigate the potential presence of amino acid or carbamates within the precipitates, 10 mg precipitate was added in the mixed solvent of 700 μL D_2O and 15 μL 1,4 dioxane, and the upper solvent was used for NMR analysis. In the ^{13}C NMR spectra, the peak, corresponding to HCO_3^-/CO_3^{2-}, shifted from 168 ppm to 161 ppm. The spectral signals of carbamate were identified as peaks at 46 ppm (CH_2), 165 ppm (C = O), and 180 ppm (C = O). The spectra also revealed shifts of peaks for Gly, from 182 to 174 ppm (C = O) and from 45 to 42 ppm (CH_2). The peak

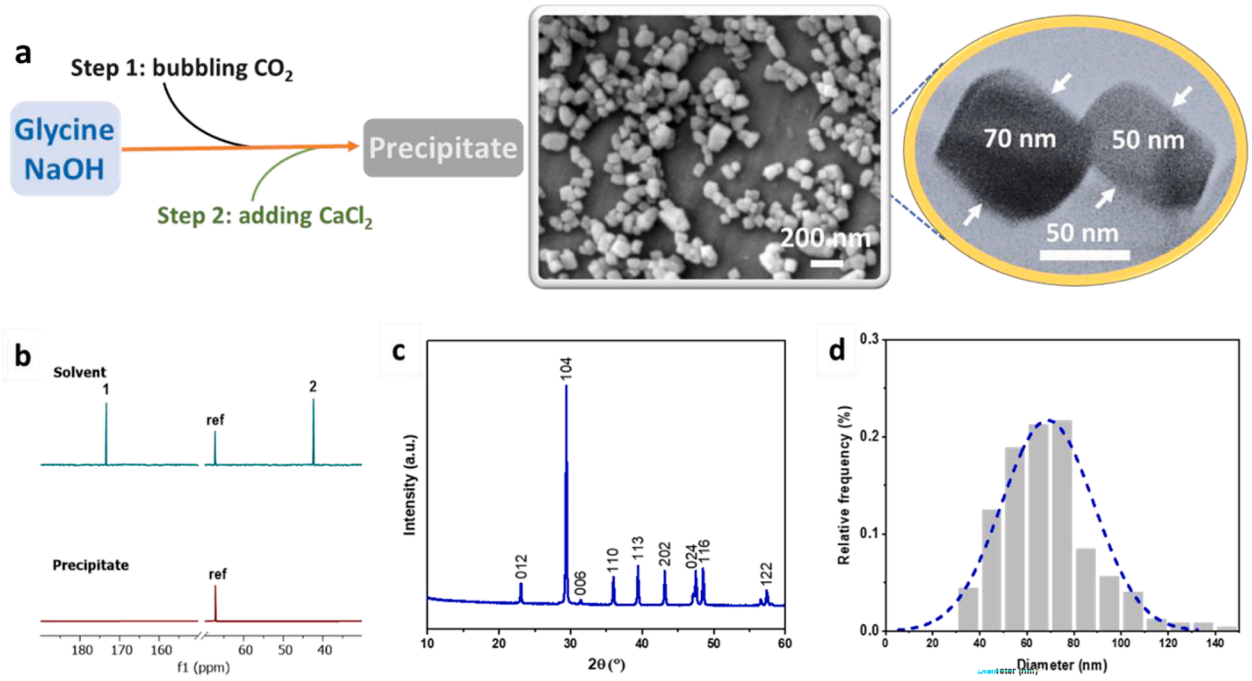

Fig. 2. a) an innovative two-step process capturing and converting CO_2 into nano-$CaCO_3$. b) NMR spectra of solvent and the precipitates after the two-step process. c) XRD spectra of the produced nano-$CaCO_3$. d) size distribution from SEM images of the produced nano-$CaCO_3$ (480 particles in 4 images). Experimental conditions: Gly (0.05 mol), NaOH (0.05 mol), $CaCl_2$ (0.05 mol), CO_2 gas flow rate (100 sccm), and CO_2 bubbling time (20 min).

corresponding to 1,4-dioxane at 67.19 ppm served as a reference but was excluded from the analysis to ensure a focus on the solutes of interest.

^{13}C NMR spectroscopy also provides a means to quantify the concentration of each chemical species in the solvent based on the area of the respective NMR peaks. In our solvent system, amino acid can transform into carbamate. The percentages of carbamate and Gly/Gly^- were calculated from the NMR spectra (Supplementary materials **S.1**).

2.3.2. Electron microscopy

The solid precipitates after vacuum drying were distributed onto a stainless-steel disc and were coated with gold using a Denton Desk V Sputter Coater for 240 sec at an 18-mA current in N_2. The precipitates were imaged using a JEOL JSM-7600F Scanning Electron Microscope (SEM). Images were captured at an acceleration voltage of 5 kV and a working distance of ~ 15 mm. Transmission Electron Microscopy (TEM) was also used to visualize the precipitates using a JEOL JEM-2100 TEM at an operating voltage of 120 kV; samples were prepared by suspending the precipitates in ethanol and then depositing them onto a copper grid. ImageJ was employed to analyze the sizes and size distribution of the particles using the electron microscopy images.

2.3.3. X-ray Diffraction (XRD)

XRD analysis of the precipitates was carried out using a PANalytical X'Pert Pro diffractometer, equipped with a copper Kα radiation source. The operational settings were maintained at 40 kV and 25 mA, and utilized a LynxEye detector for enhanced sensitivity and resolution. Diffraction patterns were systematically recorded over a 2θ angle range from 5 to 80 degrees.

2.3.4. Statistical analysis

The statistical analyses were carried out utilizing JMP/V16 software by SAS Institute in Cary, NC. Determination of statistical significance, set at a p-value of less than 0.05, was achieved through an analysis of variance coupled with the application of Tukey's HSD test.

3. Results

In this study, a universal method was developed to absorb and convert CO_2 into carbonate nanoparticles or nano-carbonates (nano-$CaCO_3$, nano-$BaCO_3$, and nano-Ag_2CO_3) (Fig. 1). First, amino acid salt solvents were prepared by dissolving a base and an amino acid in water, and then CO_2 was bubbled into the solvent for a certain time. Next, metal ions (Ca^{2+}, Ba^{2+}, Ag^+) were added into the solvent to mineralize the absorbed CO_2 into nano-carbonates.

3.1. Converting CO_2 into $CaCO_3$ nanoparticles using a two-step process

A two-step process was developed to convert CO_2 into nano-$CaCO_3$ (Fig. 2**a**). In the first step, CO_2 was bubbled into a Gly salt solvent. In the second step, $CaCl_2$ was added which led to the formation of solid precipitates (Supplementary materials **S.2**). SEM and TEM observations found that the precipitates were nanoparticles (Fig. 2**a**). NMR data (Fig. 2**b**) showed no signals of carbon-containing species within the precipitates and only Gly was shown in the solvent. Characterization of the precipitates found that the precipitates were pure calcite (JCPDS Card No. 86–2340), the most stable form of $CaCO_3$ (Fig. 2**c**), and the precipitates had an average diameter of approximately 70 nm (Fig. 2**d** and Supplementary materials **S.3**).

3.1.1. Comparison between the conversion of CO_2 into $CaCO_3$ with and without amino acid

The role of amino acid in converting CO_2 into $CaCO_3$ using the two-step process was examined. It was found that, in the absence of Gly, micro-sized, dense $CaCO_3$ particles (~2 μm) were formed (Fig. 3**a**); in comparison, $CaCO_3$ nanoparticles (~70 nm) were formed in the presence of Gly (Fig. 3**b**). This finding suggests that Gly played a critical role in controlling the size of the final products.

NMR data (Fig. 3**c**) showed that, in the absence of amino acids, CO_3^{2-}/HCO_3^- was formed within 2.5 min of CO_2 bubbling and their peak position in the NMR spectra shifted slightly toward lower ppm with increasing CO_2 bubbling time; the peak of CO_3^{2-}/HCO_3^- disappeared immediately upon addition of $CaCl_2$. In the presence of amino acid (i.e.,

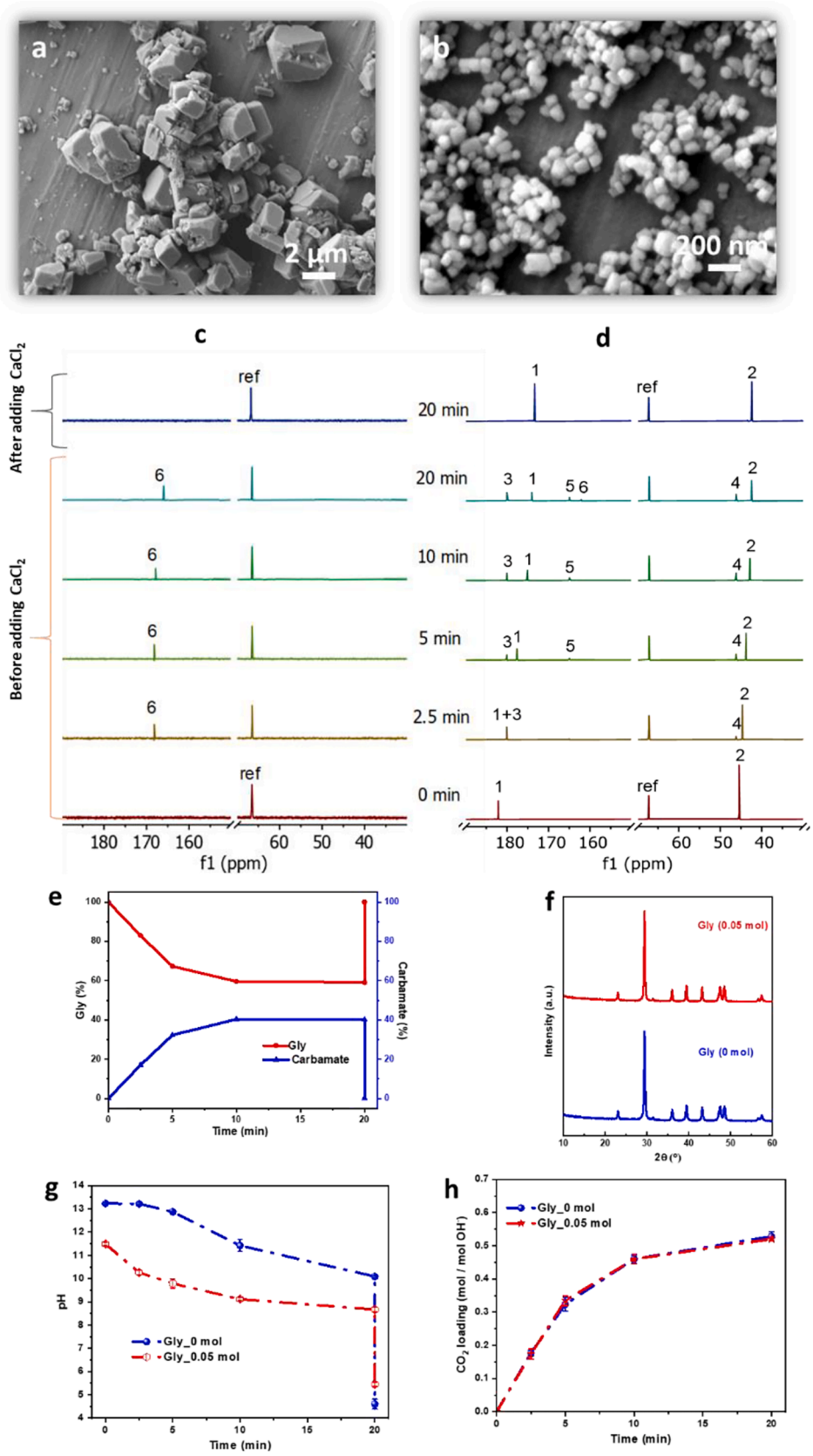

Fig. 3. SEM images of $CaCO_3$ produced a) without and b) with Gly. NMR spectra c) without and d) with Gly. e) Gly and carbamate percentages at different CO_2 bubbling times with Gly. f) XRD spectra without and with Gly. g) pH changes without and with Gly. h) CO_2 loading without and with Gly. In the spectra in c and d, peaks 1 and 2 represent Gly/Gly^-, peaks 3, 4, and 5 represent carbamate, and peak 6 represents CO_3^{2-}/HCO_3^-. 1,4-dioxane was used as the control reference (ref). Experimental conditions: Gly (0 or 0.05 mol), NaOH (0.05 mol), $CaCl_2$ (0.05 mol), CO_2 gas flow rate (100 sccm), and CO_2 bubbling time (20 min).

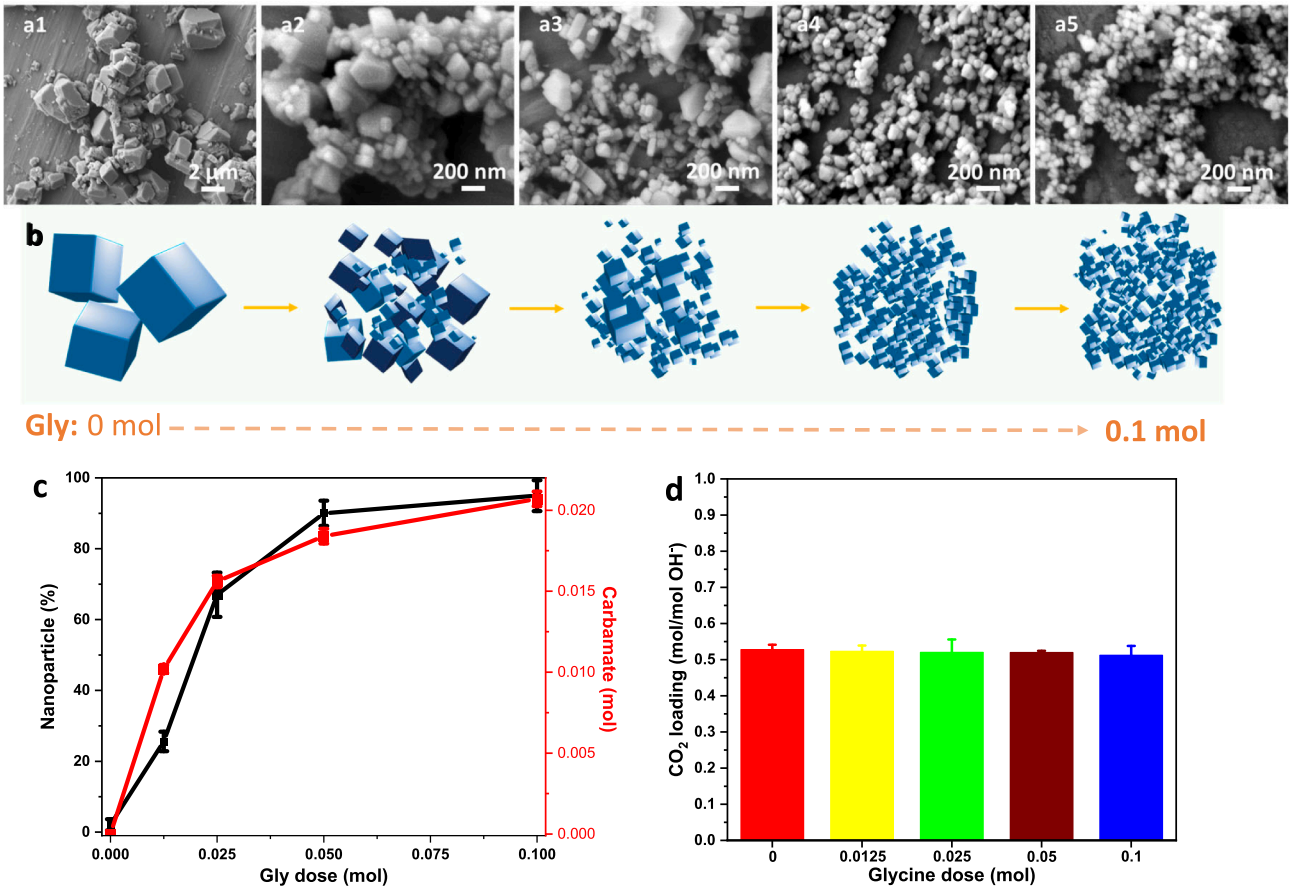

Fig. 4. a) precipitates produced using different doses of Gly (0 mol, 0.0125 mol, 0.025 mol, 0.05 mol, and 0.1 mol). b) Schematic diagram describing the evolution of particles with Gly dose. c) Percentage of nanoparticles produced at different doses of Gly, and carbamate amount at 20 min at different doses of Gly before adding $CaCl_2$. d) CO_2 loading after bubbling CO_2 for 20 min. Experimental conditions: Gly (0–0.1 mol), NaOH (0.05 mol), $CaCl_2$ (0.05 mol), CO_2 gas flow rate (100 sccm), and CO_2 bubbling time (20 min).

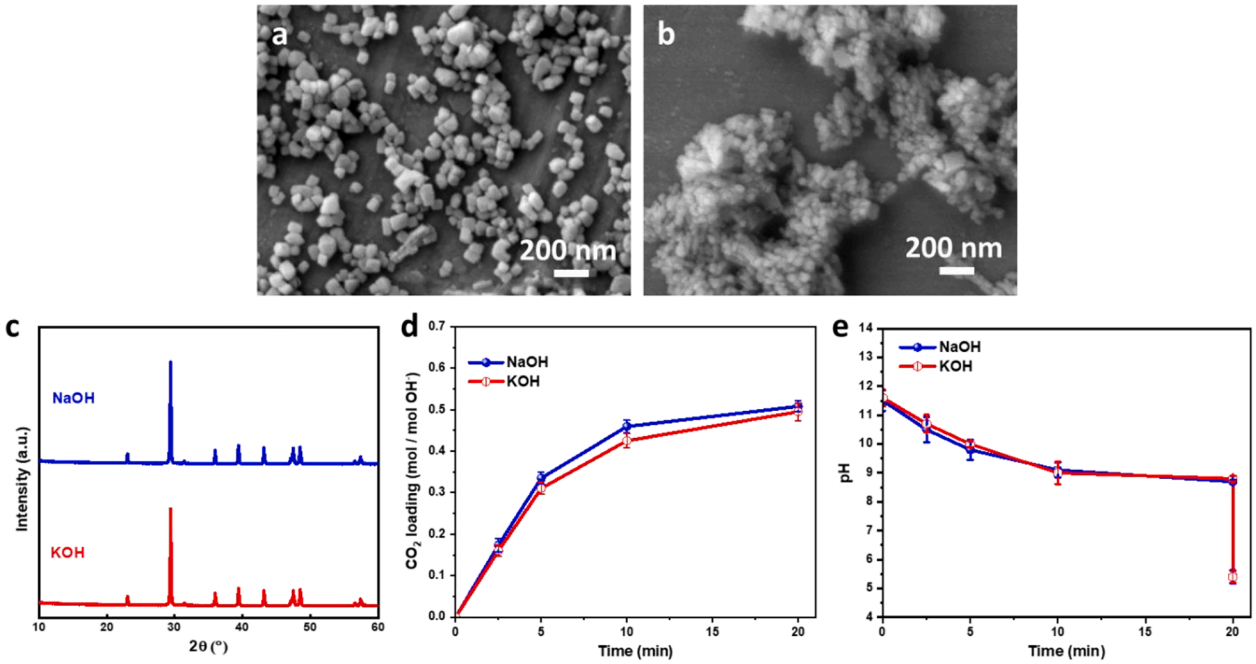

Fig. 5. Nano-$CaCO_3$ prepared from a) NaOH and b) KOH as the base. c) XRD spectra of nano-$CaCO_3$. d) CO_2 loading before and after $CaCl_2$ addition. e) pH changes before and after $CaCl_2$ addition. Experimental conditions: Gly (0.05 mol), KOH (0.05 mol), NaOH (0.05 mol), $CaCl_2$ (0.05 mol), CO_2 gas flow rate (100 sccm), and CO_2 bubbling time (20 min).

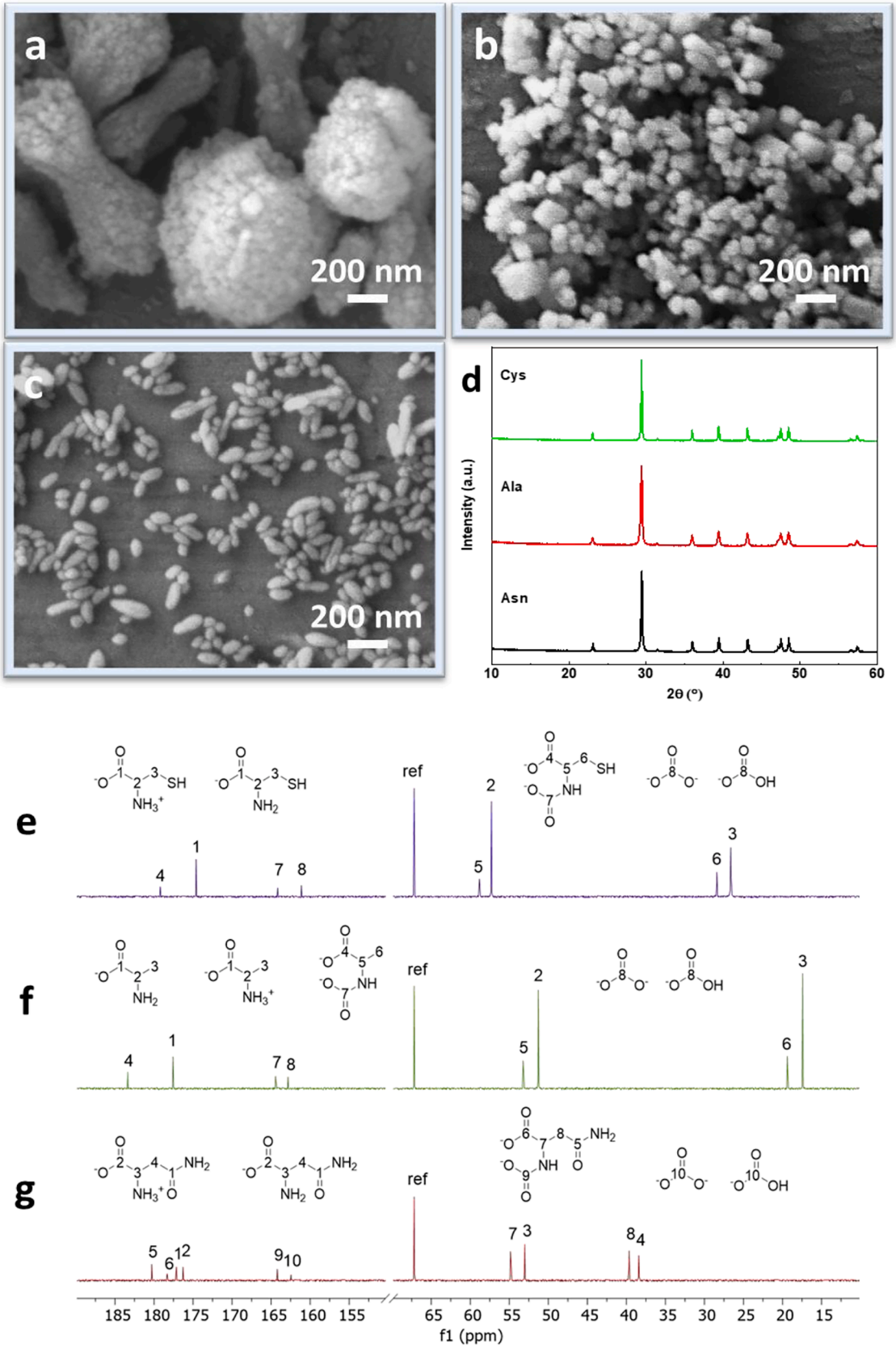

Fig. 6. Nano-$CaCO_3$ prepared from a) Asn, b) Ala, and c) Cys. d) XRD spectra of the nanoparticles prepared from various amino acids. ^{13}C NMR spectra of solvent bubbled CO_2 for 20 min with e) Cys, f) Ala, g) Asn, respectively. The peak numbers in the spectra are from molecular structures (insets). Experimental conditions: Asn (0.05 mol), Ala (0.05 mol), Cys (0.05 mol), NaOH (0.05 mol), $CaCl_2$ (0.05 mol), CO_2 gas flow rate (100 sccm), and CO_2 bubbling time (20 min).

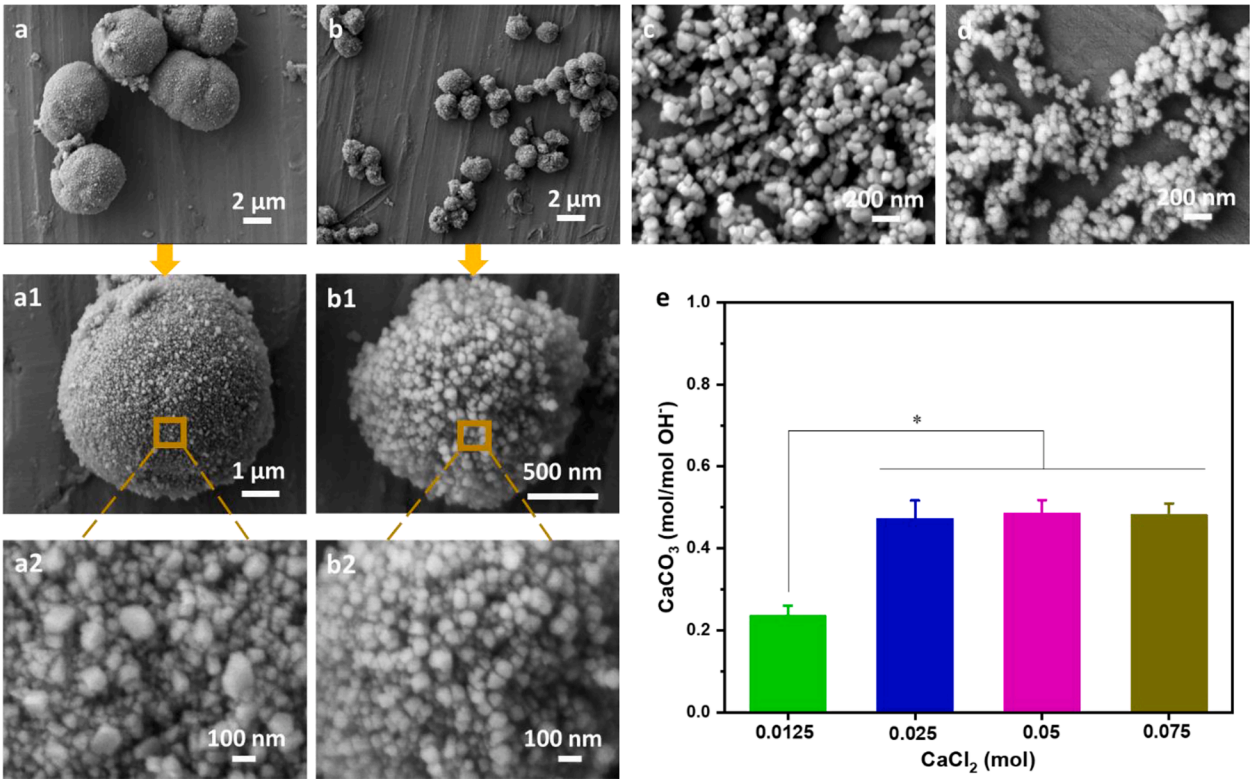

Fig. 7. Formation of $CaCO_3$ nanoparticles at various doses of $CaCl_2$ at a) 0.0125 mol, b) 0.025 mol, c) 0.05 mol, and d) 0.075 mol. a1, a2, b1, and b2 were at higher magnifications compared to a and b, respectively. e) Molar ratio of $CaCO_3$ produced to NaOH added. Experimental conditions: Gly (0.05 mol), NaOH (0.05 mol), $CaCl_2$ (0.0125–0.075 mol), CO_2 gas flow rate (100 sccm), and CO_2 bubbling time (20 min). *$p < 0.05$.

Gly), by contrast, carbamate was first formed and CO_3^{2-}/HCO_3^- appeared at 20 min; upon addition of $CaCl_2$, both carbamate and CO_3^{2-}/HCO_3^- disappeared and only the peaks for Gly/Gly^- were observed (Fig. 3**d**). The percentage of carbamate increased sharply within the first 10 min and remained about the same until 20 min then dropped to 0 upon addition of $CaCl_2$. In contrast, percentage of Gly decreased quickly within 10 min and then kept consistent at 20 min, and finally rose to 100 % upon the addition of $CaCl_2$ (Fig. 3**e**). These NMR data clearly indicated that the chemical reactions during the two-step process were different between the solvents with and without amino acid (i.e., Gly), though XRD (Fig. 3**f**) confirmed that the converted solid products were pure calcites with or without amino acid.

Meanwhile, dramatic differences in pH change were observed between the two solvents with and without Gly (Fig. 3**g**). In the absence of Gly, the pH was 13.2 before CO_2 bubbling which decreased with increasing CO_2 bubbling time and dropped to 10.1 at 20 min. Upon addition of $CaCl_2$, the pH immediately further dropped to 4.6. In comparison, in the presence of Gly, the pH was 11.5 before CO_2 bubbling and it also decreased with increasing CO_2 bubbling time and became 8.7 at 20 min; with the addition of $CaCl_2$, the pH immediately dropped to 5.5.

In addition, the CO_2 loading for the two solvents with and without Gly was almost identical; both were approximately 0.5 mol CO_2/(mol OH^-) after bubbling CO_2 for 20 min (Fig. 3**h**).

3.1.2. *Competition between the formation of nanoparticles and microparticles*

It was further revealed that the morphology of particles changed dramatically with the increasing dose of Gly, as illustrated in Fig. 4**a**. It was proposed in Fig. 4**b** that microparticles tended to form in the absence of Gly, while nanoparticles would form in the presence of Gly. Both nanoparticles and microparticles were formed and co-existed at 0.0125 mol (Fig. 4**a2**) and 0.025 mol (Fig. 4**a3**) Gly. The percentage of nanoparticles increased with increasing Gly concentration in the range of 0 to 0.05 mol (Fig. 4**c**); note that the CO_2 conversion at 0 to 0.05 mol Gly was about the same (Fig. 4**d**). The formation of nanoparticles directly correlated to the amount of carbamate formed; the more carbamate formation, the more formation of nanoparticles (Fig. 4**c**). It was clear that in the absence of amino acid (i.e., Gly), microparticles were formed and it was the presence of Gly that led to the formation of nanoparticles. At relatively lower concentrations of Gly, there was a competition in the formation of nanoparticles and microparticles.

3.1.3. *Factors impacting CO_2 conversion as $CaCO_3$ nanoparticles*

The use of both NaOH (Fig. 5**a**) and KOH (Fig. 5**b**) resulted in the formation of nanoparticles; KOH seemed to have resulted in a smaller size (~50 nm) along with more aggregation (Fig. 5**b**). The XRD spectra of the precipitates were identical for the use of both NaOH and KOH, demonstrating that the solid precipitates obtained were calcite (Fig. 5**c**). Furthermore, the CO_2 loading (Fig. 5**d**) and pH profiles (Fig. 5**e**) of the two solvents were almost identical for both NaOH and KOH before and after $CaCl_2$ was added. The CO_2 loading increased with increasing CO_2 bubbling time and reached about 0.5 mol CO_2/(mol OH^-) at 20 min; no significant changes in CO_2 loading were observed before or after $CaCl_2$ was added (Fig. 5**d**). The pH of the solvent decreased with increasing time from 11.5 at 0 min to 8.7 at 20 min, and a sharp drop in pH was observed immediately upon the addition of $CaCl_2$; the pH dropped to about 5.5 and remained steady thereafter (Fig. 5**e**).

Besides Gly, three additional amino acids including Asn, Ala, and Cys were assessed; they were selected to represent amino acids with polar uncharged side chains, amino acids with hydrophobic side chains, and amino acids with a unique side chain like −SH, respectively. All the amino acids studied resulted in the formation of nano-$CaCO_3$ using our two-step process (Fig. 6). Compared to the nano-$CaCO_3$ formed from Gly (Fig. 2**a**), Asn and Ala formed similarly shaped nanoparticles, although the nanoparticles from Asn had more aggregation and were aggregated into large porous particles like those bone-like ones (Fig. 6**a**) and the

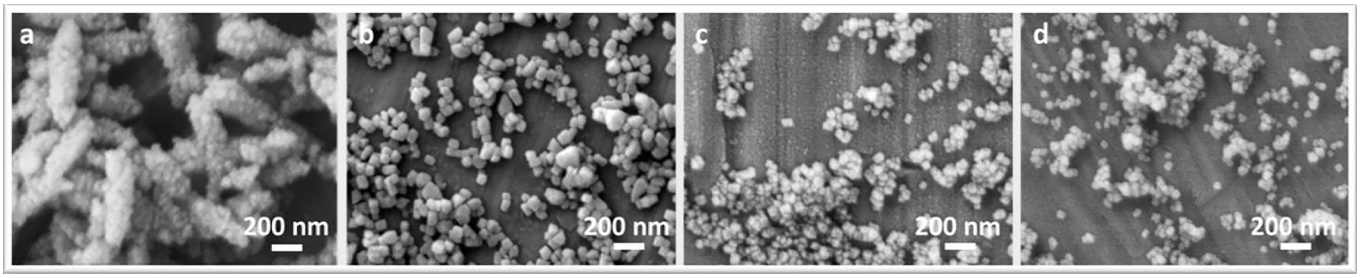

Fig. 8. SEM images of $CaCO_3$ nanoparticles formed at a) Gly:NaOH:$CaCl_2$ = 0.025 mol:0.025 mol:0.025 mol, b) Gly:NaOH:$CaCl_2$ = 0.050 mol:0.050 mol:0.050 mol, c) Gly:NaOH:$CaCl_2$ = 0.075 mol:0.075 mol:0.075 mol, and d) Gly:NaOH:$CaCl_2$ = 0.100 mol:0.100 mol:0.100 mol. Experimental conditions: Gly (0.025–0.100 mol), NaOH (0.025–0.100 mol), $CaCl_2$ (0.025–0.100 mol), CO_2 gas flow rate (100 sccm), and CO_2 bubbling time (20 min).

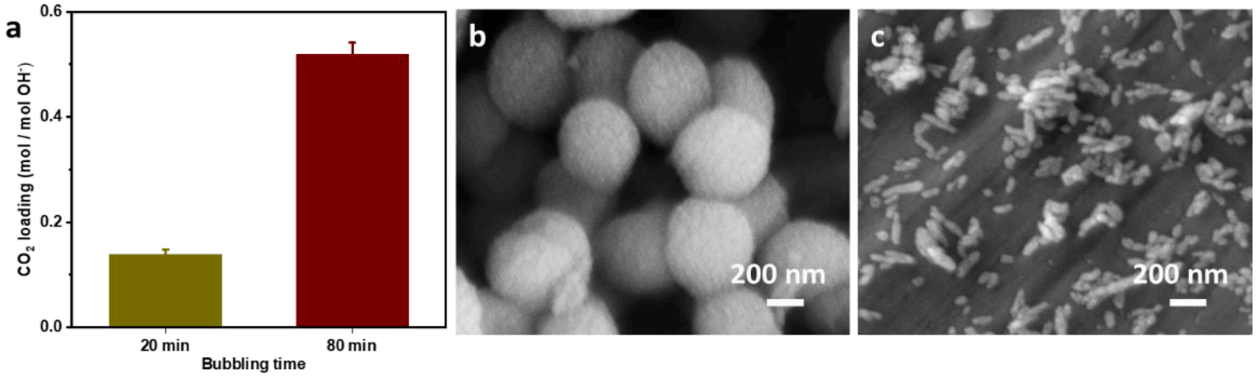

Fig. 9. Synthesis of nano-$CaCO_3$ using diluted CO_2 (10 %). a) CO_2 loading when bubbling diluted CO_2 for 20 min and 80 min. SEM of $CaCO_3$ produced after bubbling diluted CO_2 for b) 20 min and c) 80 min. d) XRD of nano-$CaCO_3$. Experimental conditions: Gly (0.05 mol), NaOH (0.05 mol), $CaCl_2$ (0.05 mol), diluted CO_2 gas flow rate (100 sccm, CO_2 10 scc L m & N_2 90 sccm).

nano-$CaCO_3$ from Ala had a larger size distribution (Fig. 6**b**). The use of Cys led to the formation of ellipsoidal nanoparticles whose diameter was in the range of 20–70 nm and the ratio of length to diameter was between 1 and 3 (Fig. 6**c**). In addition, compared to doses of 0 and 0.05 mol, the 0.025 mol dose produced $CaCO_3$ with a particle size intermediate between those obtained using 0 and 0.05 mol of Asn, Ala, and Cys, respectively (**Fig. S4**). XRD spectra data confirmed that all the nanoparticles were pure calcite (Fig. 6**d**). NMR data showed that all the amino acids studied including Gly had similar NMR spectra where carbamate was observed after bubbling CO_2 for 20 min (Fig. 6**e, 6f, and 6 g**).

SEM images revealed that the $CaCl_2$ concentration significantly affected the aggregation of nano-$CaCO_3$ (Fig. 7). Close examination of the precipitates found that, at lower $CaCl_2$ concentrations (e.g., 0.0125 mol and 0.025 mol), the nano-$CaCO_3$ aggregated into micro-sized porous particles which were about 4–6 μm at 0.0125 mol (Fig. 7**a**) and 1–2 μm at 0.025 mol (Fig. 7**b**). The shape and size of the nanoparticles formed at 0.05 mol (Fig. 7**c**) and 0.075 mol (Fig. 7**d**) were similar. Quantitative analysis showed that the molar ratio of $CaCO_3$ produced to OH^- added was approximately 0.25 mol $CaCO_3$/(mol OH^-) at 0.0125 mol $CaCl_2$ and increased to about 0.5 mol $CaCO_3$/(mol OH^-) at 0.025–0.075 mol $CaCl_2$ (Fig. 7**e**).

When keeping the molar ratio of Gly:NaOH:$CaCl_2$ constant at 1:1:1, the size of the $CaCO_3$ nanoparticles seemed to decrease slightly with increasing concentrations of the reactants (Fig. 8), suggesting that higher concentrations of reactants favor the formation of smaller nanoparticles. Interestingly, corn-shaped nanoparticles (~200 nm in diameter and 600 nm in length) were formed via aggregations at low reactant concentrations (i.e., Gly:NaOH:$CaCl_2$ = 0.025 mol:0.025 mol:0.025 mol).

3.1.4. Converting CO_2 as $CaCO_3$ nanoparticles using simulated flue gas

A simulated flue gas (10 % CO_2; 10 sccm CO_2 and 90 sccm N_2) was studied. After bubbling the solvent with the simulated flue gas for 20 min, the CO_2 loading was 0.14 mol/mol OH^- (Fig. 9**a**) and the particles were approximately 400 nm (Fig. 9**b**). After increasing the gas bubbling time to 120 min, the CO_2 loading increased to 0.52 mol/mol OH^- (Fig. 9**a**) and the particles formed were approximately 50 nm (Fig. 9**c**).

3.2. Converting CO_2 into other nano-carbonates (i.e., $BaCO_3$, Ag_2CO_3) using a two-step process

Besides the nano-$CaCO_3$, other carbonates like $BaCO_3$ and Ag_2CO_3 were produced to demonstrate the universal use of the developed method. All experimental conditions were kept the same as those for nano-$CaCO_3$ synthesis except that $CaCl_2$ was replaced by $BaCl_2$ and $AgNO_3$ to produce nano-carbonates using the two-step method. It was shown (Fig. 10**a** and 10**b**) that both precipitates had at least one dimension smaller than 100 nm. Fig. 10**a** showed that the nano-$BaCO_3$ were rods with diameters of approximately 50 nm (average from 100 particles; sizes varying from 30-90 nm) and ratios of diameter to length from 1:1 to 1:4. Fig. 10**b** showed that the obtained nano-Ag_2CO_3 were spherical shaped with small diameters of about 7 nm (varying from 5-10 nm). XRD spectra confirmed that those precipitates were $BaCO_3$ (JCPDS No. 05–0378)[22] (Fig. 10**c**) and Ag_2CO_3 (JCPDS No. 31–1236) [23,24] (Fig. 10**d**).

3.3. Converting CO_2 into nanoparticles via a one-step process

The feasibility of a one-step process for CO_2 conversion into nano-$CaCO_3$ was also investigated where Gly, NaOH, and $CaCl_2$ were mixed in water followed by CO_2 bubbling. In the absence of Gly, CO_2 loading was negligible (Fig. 11**a**), and the pH of the solution remained around 11.0

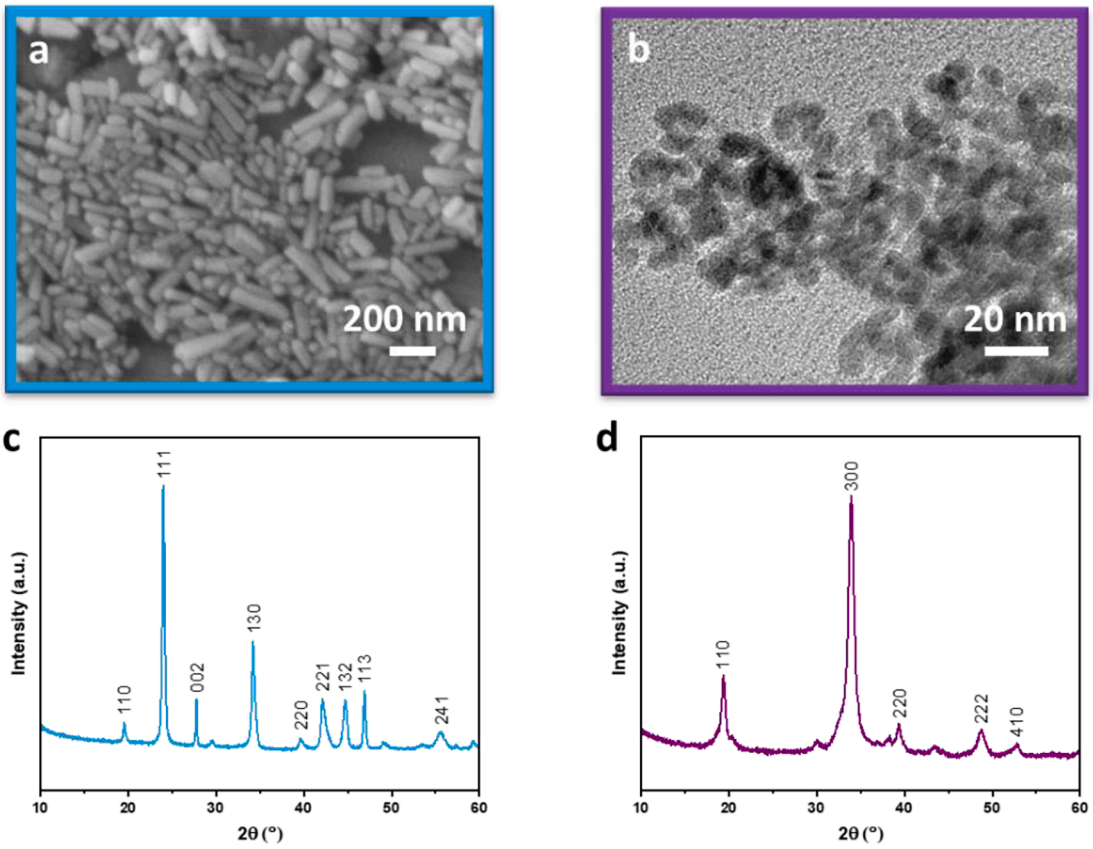

Fig. 10. Two-step process converting CO_2 into various carbonate nanoparticles. a-b) SEM of precipitates produced by $BaCl_2$ and $AgNO_3$, respectively. c-d) XRD of precipitates produced by $BaCl_2$ and $AgNO_3$, respectively. Experimental conditions: Gly (0.05 mol), NaOH (0.05 mol), $BaCl_2$(0.05 mol), $AgNO_3$(0.05 mol), CO_2 gas flow rate (100 sccm), and CO_2 bubbling time (20 min).

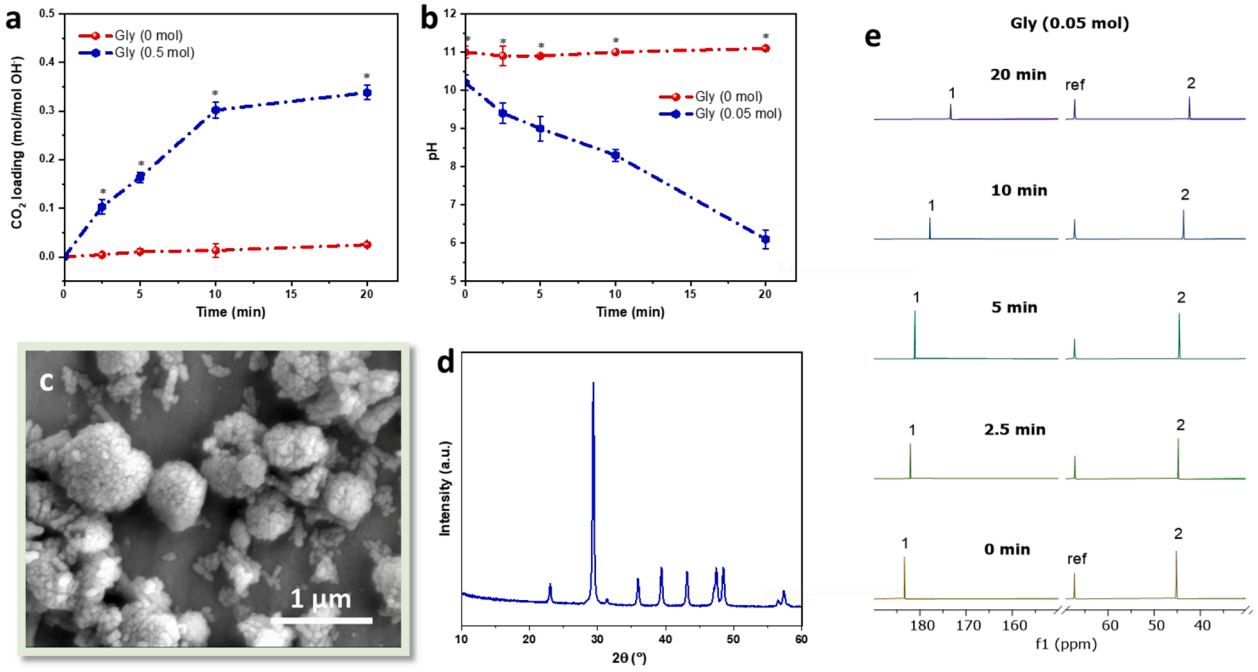

Fig. 11. Synthesis of nano-$CaCO_3$ via the one-step process where a solvent with Gly, NaOH, and $CaCl_2$ was mixed and followed by CO_2 bubbling. a) CO_2 loading *vs.* CO_2 bubbling time with and without Gly. b) pH changes *vs.* CO_2 bubbling time with and without Gly. c) SEM of nano-$CaCO_3$ produced after bubbling CO_2 for 20 min. d) XRD of nano-$CaCO_3$. e) NMR *vs.* CO_2 bubbling time with Gly. Experimental conditions: Gly (0 or 0.05 mol), NaOH (0.05 mol), $CaCl_2$ (0.05 mol), CO_2 gas flow rate (100 sccm), and CO_2 bubbling time (20 min). *$p < 0.05$ compared to the control at the same CO_2 bubbling time.

during the CO_2 bubbling process (Fig. 11**b**). By contrast, Gly (0.05 mol) addition to the solvent before CO_2 bubbling significantly enhanced CO_2 loading, and with increasing CO_2 bubbling time, CO_2 loading increased almost linearly between 0 and 10 min followed by a slow increase that led to a CO_2 loading of 0.34 mol/mol OH^- at 20 min (Fig. 11**a**). Meanwhile, pH of the solvent with Gly decreased from 10.2 to 6.1 from time 0 to 20 min (Fig. 11**b**). After bubbling CO_2 for 20 min, nano-$CaCO_3$ was formed, and the majority of which aggregated into bigger particles with several hundred nanometers (Fig. 11**c**). XRD data showed calcite was the only product (Fig. 11**d**). With increasing CO_2 bubbling time, the peaks of Gly in the NMR spectra shifted while no other new peaks were observed; no peaks for carbamate or CO_3^{2-}/HCO_3^- were observed throughout the one-step process (Fig. 11**e**).

4. Discussion

We have developed innovative processes based on amino acids to convert CO_2 into various nano-carbonates with average diameters of 7 nm, 50 nm, and 70 nm. Our method is energy-saving as it was conducted under ambient room conditions with no heat and pressure required. The production of nano-carbonates from CO_2 is significant, because it not only converts CO_2 into carbonates that are stable, but the smaller size and higher surface area make nano-carbonates more attractive compared to large-sized particles.

The global nanomaterials market, valued at approximately US$ 12.5 billion in 2023, is projected to grow at a 15.0 % CAGR from 2024 to 2030 [11]. Growth is mainly driven by increased demand in electronics and expanding applications in the medical industry. Carbonate (e.g., $CaCO_3$, $BaCO_3$, Ag_2CO_3) nanomaterials have been or potentially can be used as fillers, medicines, catalysts, and in various sectors such as industry (food, construction, paint, polymer), biomedical, environmental, and electronic fields. For example, $CaCO_3$ nanoparticles have been widely used in plastics, rubber, paint, and paper industries as an enhancer and filler [25,26]. $BaCO_3$ nanoparticles can be used in the manufacture of electronic ceramic materials such as high dielectric constant ceramics in capacitors and inductors [27,28]. Ag_2CO_3 nanomaterials can be used as antibacterial agents [29,30] and photocatalysts [31,32]. Moreover, the universal approach developed in this study can be applied to produce other carbonate nanoparticles like $SrCO_3$, $MgCO_3$, $FeCO_3$, $MnCO_3$, $CuCO_3$, and so on. Nanoparticles like $SrCO_3$ alone had a market value of US$ 220 million in 2023 which may reach US$ 340 million by 2030 [33,34].

This study clearly demonstrated that it was the amino acid (e.g., Gly) that dictated the formation of nano-carbonates. The formation of $CaCO_3$ was used as an example to illustrate the nanoparticle formation mechanism. The sizes of the produced $CaCO_3$ were dramatically different in the presence and absence of amino acid. In the absence of amino acid, microparticles (~ 2 μm) were formed while nanoparticles (~ 70 nm) were formed in the presence of Gly in the same process (Fig. 3**a and 3b**). Our NMR data clearly showed that in the presence of Gly, carbamate was formed first within minutes after CO_2 bubbling and HCO_3^- appeared later, e.g., 20 min after CO_2 bubbling (Fig. 3**d**). Meanwhile, the pH of the solvent decreased with increasing CO_2 bubbling time (Fig. 3**g**). Our NMR findings indicated that Gly reacted with CO_2 to form carbamate, which subsequently hydrolyzed into HCO_3^-, which further partially converted to CO_3^{2-}; these findings, along with the pH change, were consistent with previous studies where amino acids were used for CO_2 absorption [20,35–41]. Upon addition of $CaCl_2$ in our two-step process, both carbamate and HCO_3^- disappeared and only the peaks for Gly/Gly^- were observed (Fig. 3**d**). The pH of the solvent dropped significantly (Fig. 3**g**), and formation of pure nano-$CaCO_3$ was confirmed via XRD (Fig. 2**c and 3f**). These results suggested that carbamate completely hydrolyzed and Ca^{2+} reacted with HCO_3^-/CO_3^{2-} to form $CaCO_3$ as shown below.

In the presence of amino acids:

Before CO_2 bubbling

$$^{+}H_3NCH_2COO^- + OH^- \rightleftarrows H_2NCH_2COO^- + H_2O$$

During CO_2 bubbling

$$CO_2 + 2H_2NCH_2COO^- \rightleftarrows {}^{-}OOC\text{-}HNCH_2COO^- + {}^{+}H_3NCH_2COO^-$$

$$^{-}OOC\text{-}HNCH_2COO^- + H_2O \rightleftarrows H_2NCH_2COO^- + HCO_3^-$$

$$^{+}H_3NCH_2COO^- + OH^- \rightleftarrows H_2NCH_2COO^- + H_2O$$

$$CO_2 + OH^- \rightleftarrows HCO_3^-$$

$$HCO_3^- + OH^- \rightleftarrows CO_3^{2-} + H_2O$$

After $CaCl_2$ added

$$^{-}OOC\text{-}HNCH_2COO^- + H_2O \rightleftarrows H_2NCH_2COO^- + HCO_3^-$$

$$^{+}H_3NCH_2COO^- + OH^- \rightleftarrows H_2NCH_2COO^- + H_2O$$

$$Ca^{2+} + CO_3^{2-} \Rightarrow CaCO_3\downarrow$$

$$HCO_3^- + Ca^{2+} + OH^- \Rightarrow CaCO_3\downarrow + H_2O$$

In the absence of amino acids, HCO_3^-/CO_3^{2-} was observed in the same two-step process during CO_2 bubbling (Fig. 3**c**); with the addition of $CaCl_2$, the pH of the solvent dropped sharply (Fig. 3**g**) and $CaCO_3$ microparticles were formed immediately (Fig. 3**a**). These findings were consistent with the traditional method of production of $CaCO_3$ through the following reactions:

In the absence of amino acids:

During CO_2 bubbling

$$CO_2 + OH^- \rightleftarrows HCO_3^-$$

$$HCO_3^- + OH^- \rightleftarrows CO_3^{2-} + H_2O$$

After $CaCl_2$ added

$$Ca^{2+} + CO_3^{2-} \Rightarrow CaCO_3\downarrow$$

$$HCO_3^- + Ca^{2+} + OH^- \Rightarrow CaCO_3\downarrow + H_2O$$

Meanwhile, at relatively low concentrations of Gly (i.e., molar ratio of Gly/OH^- < 1) (Fig. 4**a2** and 4**a3**), both nanoparticles and microparticles were formed, indicating the competition of the aforementioned two pathways (i.e., amino acid-driven nanoparticles and traditional microparticles) that led to the formation of nanoparticles and microparticles, respectively. The percentage of nanoparticles increased with increasing Gly concentration and such an increase correlated with the increase of carbamate formation from Gly reacting with CO_2 (Fig. 4**c**). Therefore, it was clear that amino acids like Gly dictate the formation of nanoparticles.

Gly in the system can exist in three forms: remaining in the solvent, converted to carbamate, or adhered on $CaCO_3$ nanoparticles. In this study, after forming $CaCO_3$ nanoparticles, no carbamate was detected in the solvent and no Gly was detectable in the $CaCO_3$ precipitates (Fig. 2**b**), therefore Gly remained in the solvent and no Gly was consumed upon the formation of $CaCO_3$ nanoparticles. The Gly could be recycled and reused while additional steps may be necessary to address the buildup of Na^+ and Cl^- ions in the solution in the cyclic uses. Various methods for separating Na^+ and Cl^- are available [42] and we may investigate strategies to avoid the formation of such ions in the future.

Various experimental factors may influence the size and shape of the nanoparticles formed. These factors may include the Gly concentration (Fig. 4**)**, different bases (Fig. 5**)**, type of amino acids (Fig. 6**)**, $CaCl_2$ concentration (Fig. 7**)**, and whole solvent concentration (Fig. 8**)**. Among these, the dose of Gly appeared to be the most critical. Particle size decreased with an increase in Gly concentration and when it exceeded 0.05 mol, further changes in particle size were negligible. The chemical (e.g., Ca^{2+}, Ba^{2+}, Ag^+) seemed to have played a major role in the formation of various carbonates of different nanoparticle sizes, since the $CaCO_3$, $BaCO_3$, and Ag_2CO_3 nanoparticles produced had different diameters of 70 nm, 50 nm, and 7 nm, respectively. It is possible to achieve similar sizes of different carbonate nanoparticles by optimizing the various factors mentioned above.

The method presented here was operated under mild reaction conditions and utilized readily available raw materials. By simply changing the salt used in the process, a variety of carbonate nanoparticles were produced. These advantages made the method highly suitable for industrial-scale production of various carbonate nanoparticles without requiring modifications to the procedure or additional energy input. Moreover, this method can utilize diluted CO_2 concentrations (Fig. 9) to synthesize nanoparticles, making it a promising approach for converting CO_2 from flue gases or ambient air. This conversion into value-added carbonate nanoparticles could help offset the costs associated with CO_2 management, providing both economic and environmental benefits.

In this study, two methods have been developed for the conversion of CO_2 into nano-$CaCO_3$: two-step process (Fig. 2) and one-step process (Fig. 11). Gly played a critical role in controlling the morphology of calcite in both methods (Figs. 3 and 11). In the one-step process, the presence of Gly was essential as CO_2 loading did not occur without it (Fig. 11**a**). Compared to the two-step process, the one-step approach offered greater convenience and was potentially more favorable for industrial applications because all reactants were added simultaneously at the beginning, eliminating the need to add $CaCl_2$ during the process. However, this method resulted in particle aggregation (Fig. 11**c**) and lower CO_2 loading (Fig. 11**a**). The reduced CO_2 loading in the one-step process might be due to the observation of white precipitates when Gly, NaOH, and $CaCl_2$ were mixed, theoretically resulting from the reaction between NaOH and $CaCl_2$ that produced $Ca(OH)_2$. It was clear that, in the two-step process, amino acids like Gly participated in the CO_2 absorption process and resulted in the formation of nano-$CaCO_3$. In the one-step process, although no formation of carbamate or HCO_3^- was observed, the shift of Gly peaks was similar to the two-step process (Fig. 11**e**), and the pH change was also similar (Fig. 11**b**). Therefore, it is believed that Gly also participated in the CO_2 absorption in the one-step process although the detection of carbamate and bicarbonate formation via the NMR method was not possible.

5. Conclusions

Amino acid salt solvents have been studied to capture CO_2 primarily for geological sequestration; this study, for the first time, developed innovative methods based on amino acid salt solvents to capture and convert CO_2 into different types of nano-carbonates. It was found that when bubbling CO_2 into solvents with NaOH only, HCO_3^- was formed, and $CaCO_3$ microparticles (~ 2 μm) were formed upon the subsequent addition of $CaCl_2$. Interestingly, when CO_2 was bubbled into solvents with both Gly and NaOH at a 1:1 ratio, carbamate formed first before HCO_3^- formation and $CaCO_3$ nanoparticles (~ 70 nm) were obtained when $CaCl_2$ was added. NMR data clearly showed that the volume of nanoparticles formed was directly proportional to the amount of carbamate formed. When the ratios of Gly to NaOH were less than 1:1, both nanoparticles and microparticles were formed and a competition between two different reaction pathways seemed to have occurred. In the one-step process, when $CaCl_2$ was added at the same time along with Gly and NaOH, $CaCO_3$ nanoparticles were formed. However, they were more aggregated and the CO_2 loading was relatively lower compared to the two-step process. Therefore, this study clearly demonstrated that amino acids were required for the formation of $CaCO_3$ nanoparticles and amino acids resulted in different chemical reactions as compared to the solvents without amino acids. Furthermore, the method has been proven to be universal to produce various types of nano-carbonates including nano-$CaCO_3$, nano-$BaCO_3$, and nano-Ag_2CO_3.

Declaration of competing interest

The authors declare the following financial interests/personal relationships which may be considered as potential competing interests: Bingyun Li reports financial support was provided by USDA National Institute of Food and Agriculture. Bingyun Li reports financial support was provided by WV Higher Education Policy Commission. If there are other authors, they declare that they have no known competing financial interests or personal relationships that could have appeared to influence the work reported in this paper.

Acknowledgements

This material is based upon work supported by the Agriculture and Food Research Initiative Competitive Grant (no. 2020-68012-31881) from the USDA National Institute of Food and Agriculture and by the WV Higher Education Policy Commission under grant number RCG23-12 and the WVU Internal Grant. We also acknowledge use of the WVU Shared Research Facilities. The findings and conclusions in this report are those of the authors and do not necessarily represent the official position of the National Institute for Occupational Safety and Health, Centers for Disease Control and Prevention, the funding agencies, or their institutions. The authors thank Suzanne Danley for proofreading.

Appendix A. Supplementary data

Supplementary data to this article can be found online at https://doi.org/10.1016/j.seppur.2024.131207.

Data availability

Data will be made available on request.

References

[1] D. Sivanesan, M.H. Youn, A. Murnandari, J.M. Kang, K.T. Park, H.J. Kim, S. K. Jeong, Enhanced CO_2 absorption and desorption in a tertiary amine medium with a carbonic anhydrase mimic, J. Ind. Eng. Chem. 52 (2017) 287–294, https://doi.org/10.1016/j.jiec.2017.03.058.

[2] M. Liu, G. Gadikota, Single-step, low temperature and integrated CO_2 capture and conversion using sodium glycinate to produce calcium carbonate, Fuel 275 (2020) 117887, https://doi.org/10.1016/j.fuel.2020.117887.

[3] D. Madhav, T. Coppitters, Y. Ji, W. Thielemans, F. Desplentere, P. Moldenaers, V. Vandeginste, Amino acid promoted single-step carbon dioxide capture and mineralization integrated with polymer-mediated crystallization of carbonates, J. Cleaner Prod. (2023) 137845, https://doi.org/10.1016/j.jclepro.2023.137845.

[4] C. Oeiyono, R.R. Ratnakar, K. Mohanty, Experimental investigation of amine regeneration for carbon capture through CO_2 mineralization, SPE J. 29 (10) (2024) 5702–5716, https://doi.org/10.2118/223085-PA.

[5] Y. Huang, X. Zheng, Y. Wei, Q. He, S. Yan, L. Ji, Protonated amines mediated CO_2 mineralization of coal fly ash and polymorph selection of $CaCO_3$, Chem. Eng. J. 450 (2022) 138121, https://doi.org/10.1016/j.cej.2022.138121.

[6] D. Madhav, T. Coppitters, Y. Ji, W. Thielemans, F. Desplentere, P. Moldenaers, V. Vandeginste, Amino acid promoted single-step carbon dioxide capture and mineralization integrated with polymer-mediated crystallization of carbonates, J. Cleaner Prod. 415 (2023) 137845, https://doi.org/10.1016/j.jclepro.2023.137845.

[7] N. Baig, I. Kammakakam, W. Falath, Nanomaterials: A review of synthesis methods, properties, recent progress, and challenges, Mater. Adv. 2 (6) (2021) 1821–1871, https://doi.org/10.1039/D0MA00807A.

[8] M. Rafique, M.B. Tahir, M.S. Rafique, M. Hamza, History and fundamentals of nanoscience and nanotechnology, in: M.B. Tahir, M. Rafique, M.S. Rafique (Eds.), Nanotechnology and Photocatalysis for Environmental Applications, Elsevier, 2020, pp. 1–25, https://doi.org/10.1016/B978-0-12-821192-2.00001-2.

[9] S. Malik, K. Muhammad, Y. Waheed, Nanotechnology: A revolution in modern industry, Molecules 28 (2) (2023) 661, https://doi.org/10.3390/molecules28020661.

[10] Market Research Community, Nano Calcium Carbonate Market Size, Share & Trends Analysis, By Application (Plastics, Rubber, Building & Construction, Others), By Region and Forecast Period 2023 – 2030. https://marketresearchcommunity.com/nano-calcium-carbonate-market/, (accessed 17 December 2024).

[11] Grand View Research, Nano Calcium Carbonate Market Size, Share & Trends Analysis Report By Application (Plastics, Rubber, Building & Construction), By Region (Asia Pacific, North America, Europe), And Segment Forecasts, 2023 - 2030. https://www.grandviewresearch.com/industry-analysis/nano-calcium-carbonate-market, (accessed 17 December 2024).

[12] P. Fadia, S. Tyagi, S. Bhagat, A. Nair, P. Panchal, H. Dave, S. Dang, S. Singh, Calcium carbonate nano-and microparticles: synthesis methods and biological applications, 3 Biotech 11 (2021) 1–30, https://doi.org/10.1007/s13205-021-02995-2.

[13] Y.-Q. Niu, J.-H. Liu, C. Aymonier, S. Fermani, D. Kralj, G. Falini, C.-H. Zhou, Calcium carbonate: controlled synthesis, surface functionalization, and nanostructured materials, Chem. Soc. Rev. 51 (18) (2022) 7883–7943, https://doi.org/10.1039/D1CS00519G.

[14] Y. Boyjoo, V.K. Pareek, J. Liu, Synthesis of micro and nano-sized calcium carbonate particles and their applications, J. Mater. Chem. A 2 (35) (2014) 14270–14288, https://doi.org/10.1039/C4TA02070G.

[15] S. El-Sheikh, S. El-Sherbiny, A. Barhoum, Y. Deng, Effects of cationic surfactant during the precipitation of calcium carbonate nano-particles on their size, morphology, and other characteristics, Colloids Surf. A 422 (2013) 44–49, https://doi.org/10.1016/j.colsurfa.2013.01.020.

[16] S.H. Sonawane, S.P. Gumfekar, S. Meshram, M.P. Deosarkar, C.M. Mahajan, P. Khanna, Combined effect of surfactant and ultrasound on nano calcium carbonate synthesized by crystallization process, Int. J. Chem. Reactor Eng. 7 (1) (2009), https://doi.org/10.2202/1542-6580.2016.

[17] M. Karimi, A. Jodaei, A. Khajvandi, A. Sadeghinik, R. Jahandideh, In-situ capture and conversion of atmospheric CO_2 into nano-$CaCO_3$ using a novel pathway based on deep eutectic choline chloride-calcium chloride, J. Environ. Manage. 206 (2018) 516–522, https://doi.org/10.1016/j.jenvman.2017.11.005.

[18] L. Xiang, Y. Xiang, Z. Wang, Y. Jin, Influence of chemical additives on the formation of super-fine calcium carbonate, Powder Technol. 126 (2) (2002) 129–133, https://doi.org/10.1016/S0032-5910(02)00047-5.

[19] I. Moulay, J. Park, Y. Yoo, Synthesis of nano-sized calcium carbonates employing molecular effect on CO_2 conversion via biodegradable chelating-system, Chem. Eng. J. 474 (2023) 145281, https://doi.org/10.1016/j.cej.2023.145281.

[20] Z. Bao, Q. Li, N.G. Akhmedov, B.A. Li, M. Xing, J. Wang, B.I. Morsi, B. Li, Innovative cycling reaction mechanisms of CO_2 absorption in amino acid salt solvents, Chem. Eng. J. Adv. (2022) 100250, https://doi.org/10.1016/j.ceja.2022.100250.

[21] Q. Li, Z. Bao, N.G. Akhmedov, B.A. Li, Y. Duan, M. Xing, J. Wang, B.I. Morsi, B. Li, Unraveling the Role of Glycine in K_2CO_3 Solvent for CO_2 Removal, Ind. Eng. Chem. Res. 61 (34) (2022) 12545–12554, https://doi.org/10.1021/acs.iecr.2c01637.

[22] X. Chen, T. Jung, J. Park, W.-S. Kim, Preparation of single-phase three-component alkaline earth oxide of (BaSrMg) O: a high capacity and thermally stable chemisorbent for oxygen separation, J. Mater. Chem. A 3 (1) (2015) 258–265, https://doi.org/10.1039/C4TA05045B.

[23] S. Guo, J. Bao, T. Hu, L. Zhang, L. Yang, J. Peng, C. Jiang, Controllable synthesis porous Ag_2CO_3 nanorods for efficient photocatalysis, Nanoscale Res. Lett. 10 (2015) 1–8, https://doi.org/10.1186/s11671-015-0892-5.

[24] J. Li, Y. Xie, Y. Zhong, Y. Hu, Facile synthesis of Z-scheme Ag_2CO_3/Ag/AgBr ternary heterostructured nanorods with improved photostability and photoactivity, J. Mater. Chem. A 3 (10) (2015) 5474–5481, https://doi.org/10.1039/C4TA06075J.

[25] N.Q. Mahmood, M. Hikmat, The effect of calcium carbonate-nanoparticle on the mechanical and thermal properties of polymers utilizing different types of mixing and surface pre-treatment: a review paper, Eng. Technol. 41 (12) (2023) 1497–1515, https://doi.org/10.30684/etj.2023.142219.1523.

[26] H. Sharma, D.K. Ashish, Nano $CaCO_3$ for enhancing properties of cement-based materials: A comprehensive review, J. Sustainable Cem.-Based Mater. 12(12) (2023) 1475-1494. https://doi.org/10.1080/21650373.2023.2233512.

[27] T. Hong, F. Chen, C. Xia, Barium carbonate nanoparticle as high temperature oxygen reduction catalyst for solid oxide fuel cell, Electrochem. Commun. 51 (2015) 93–97, https://doi.org/10.1016/j.elecom.2014.12.017.

[28] H.G. Desta, Q. Yang, D. Tian, S. Zhu, X. Lu, K. Song, Y. Yang, Y. Chen, B. Li, B. Lin, $BaCO_3$ nanoparticles-modified composite cathode with improved electrochemical oxygen reduction kinetics for high-performing ceramic fuel cells, Catalysts 12 (9) (2022) 1046, https://doi.org/10.3390/catal12091046.

[29] O. Messaoudi, I. Benamar, A. Azizi, S. Albukhaty, Y. Khane, G.M. Sulaiman, M. M. Salem-Bekhit, K. Hamdi, S. Ghoummid, A. Zoukel, Characterization of silver carbonate nanoparticles biosynthesized using marine Actinobacteria and exploring of their antimicrobial and antibiofilm activity, Mar. Drugs 21 (10) (2023) 536, https://doi.org/10.3390/md21100536.

[30] S. Sohrabnezhad, A. Pourahmad, M.M. Moghaddam, A. Sadeghi, Study of antibacterial activity of Ag and Ag_2CO_3 nanoparticles stabilized over montmorillonite, Spectrochim. Acta, Part A 136 (2015) 1728–1733, https://doi.org/10.1016/j.saa.2014.10.074.

[31] D. Lončarević, I. Vukoje, J. Dostanić, A. Bjelajac, V. Đorđević, S. Dimitrijević, J. M. Nedeljković, Antimicrobial and photocatalytic abilities of Ag_2CO_3 nano-rods, ChemistrySelect 2 (10) (2017) 2931–2938, https://doi.org/10.1002/slct.201700003.

[32] X. Yang, R. Li, Y. Wang, K. Wu, S. Chang, H. Tang, Solvent-induced controllable synthesis of recyclable Ag_2CO_3 catalysts with enhanced visible light photocatalytic activity, Ceram. Int. 42 (12) (2016) 13411–13420, https://doi.org/10.1016/j.ceramint.2016.05.119.

[33] Valuates Reports, Strontium Carbonate Nanopowder - Global Market Share and Ranking, Overall Sales and Demand Forecast 2024-2030, https://www.marketresearchreports.com/mrrpb5/strontium-carbonate-nanopowder-global-market-share-and-ranking-overall-sales-and-demand, (accessed 17 December 2024).

[34] 24 Market Reports, Global Strontium Carbonate Nanopowder Market Research Report 2024 (Status and Outlook), https://www.24marketreports.com/chemicals-and-materials/global-strontium-carbonate-nanopowder-2024-490, (accessed 17 December 2024).

[35] G. Hu, K.H. Smith, Y. Wu, S.E. Kentish, G.W. Stevens, Screening amino acid salts as rate promoters in potassium carbonate solvent for carbon dioxide absorption, Energy Fuels 31 (4) (2017) 4280–4286, https://doi.org/10.1021/acs.energyfuels.7b00157.

[36] S. Moioli, L.A. Pellegrini, M.T. Ho, D.E. Wiley, A comparison between amino acid based solvent and traditional amine solvent processes for CO_2 removal, Chem. Eng. Res. Des. 146 (2019) 509–517, https://doi.org/10.1016/j.cherd.2019.04.035.

[37] X. Wang, N.G. Akhmedov, D. Hopkinson, J. Hoffman, Y. Duan, A. Egbebi, K. Resnik, B. Li, Phase change amino acid salt separates into CO_2-rich and CO_2-lean phases upon interacting with CO_2, Appl. Energy 161 (2016) 41–47, https://doi.org/10.1016/j.apenergy.2015.09.094.

[38] A. Kasturi, J. Gabitto, C. Tsouris, R. Custelcean, Carbon dioxide capture with aqueous amino acids: Mechanistic study of amino acid regeneration by guanidine crystallization and process intensification, Sep. Purif. Technol. 271 (2021) 118839, https://doi.org/10.1016/j.seppur.2021.118839.

[39] D.J. Deka, G.G. Jang, A. Kasturi, D. Stamberga, J.K. Keum, R. Custelcean, C. Tsouris, Pronounced reduction in the regeneration energy of potassium sarcosinate CO_2 capture solvent using TiO_2, Sep. Purif. Technol. 354 (2025) 128850, https://doi.org/10.1016/j.seppur.2024.128850.

[40] A. Kasturi, J. Gabitto, G.G. Jang, J.A. Thompson, D. Stamberga, J. Seo, D.S. Sholl, S. Yiacoumi, R. Custelcean, C. Tsouris, Sub-ambient performance of potassium sarcosinate for direct air capture applications: CO_2 flux and viscosity measurements, Sep. Purif. Technol. 357 (2025) 130026, https://doi.org/10.1016/j.seppur.2024.130026.

[41] A. Jamal, A. Meisen, C.J. Lim, Kinetics of carbon dioxide absorption and desorption in aqueous alkanolamine solutions using a novel hemispherical contactor—I. Experimental apparatus and mathematical modeling, Chem. Eng. Sci. 61 (19) (2006) 6571–6589, https://doi.org/10.1016/j.ces.2006.04.046.

[42] J.C. Thunberg, R.W. Bragdon, W.P. Moore, Process for recovering glycine from sodium chloride solutions, Google Patents (1976). https://patents.google.com/patent/US3985801A/en.

Supplementary materials

Capturing and Converting CO_2 using Amino Acids as Various Commercially Valuable Nano-carbonates

Qingyang Li[a,b], Yong Qian[c], Malcolm Xing[d], Bingyun Li[a,*]

[a]Biomaterials, Bioengineering & Nanotechnology Laboratory, Department of Orthopaedics, West Virginia University, Morgantown, WV 26506, United States

[b]Department of Chemical and Biomedical Engineering, West Virginia University, Morgantown, WV 26506, United States

[c]Pathology and Physiology Research Branch, Health Effects Laboratory Division, National Institute for Occupational Safety and Health, Morgantown, WV 26505, United States

[d]Department of Mechanical Engineering, University of Manitoba, Winnipeg, MB R3T 5V6, Canada

*Corresponding author: bili@hsc.wvu.edu

S.1. Method to determine carbamate, Gly/Gly$^-$, and HCO_3^-/CO_3^{2-} in the system using Gly as amino acid

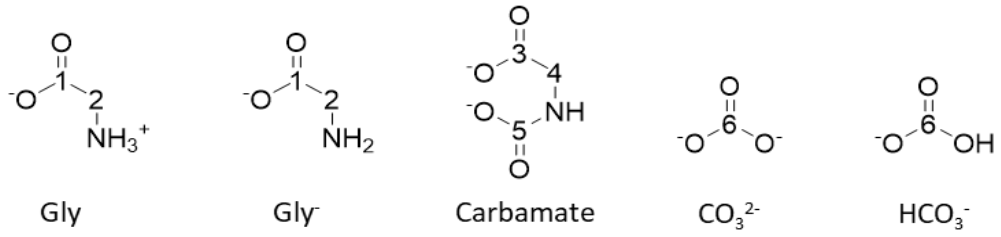

Figure S1. Numerical labeling of each carbon atom in carbamate, Gly/Gly$^-$, and HCO_3^-/CO_3^{2-}.

^{13}C NMR spectroscopy provides a means to quantify the concentration of each chemical species in the solvent, based on the area of the respective NMR peaks. In our solvent system, Gly/Gly$^-$ can only transform into carbamate. Peaks 4 and 2 were selected to represent carbamate and Gly/Gly-, respectively. Equations below were used to describe the carbamate and Gly/Gly$^-$[1-3].

$$Carbamate\ (\%) = \frac{area\ of\ peak\ 4}{area\ of\ peak\ 2 + area\ of\ peak\ 4} \times\ 100\%$$

$$Carbamate\ (mol) = Carbamate\ percentage \times Gly\ dosage$$

$$\mathrm{Gly/Gly^-}\ (\%) = 100 - Carbamate(\%)$$

S.2. Phase separation of nano-$CaCO_3$

0.05 mol Gly and 0.05 mol NaOH were mixed in 25 mL pure water used as a solvent. Subsequently, CO_2 gas was bubbled through the solvent for 20 min at a flow rate of 100 sccm. Next, 0.05 mol $CaCl_2$ was introduced into the solvent and vortexed for 1 min. After that, the sample was left to stand for 24 h.

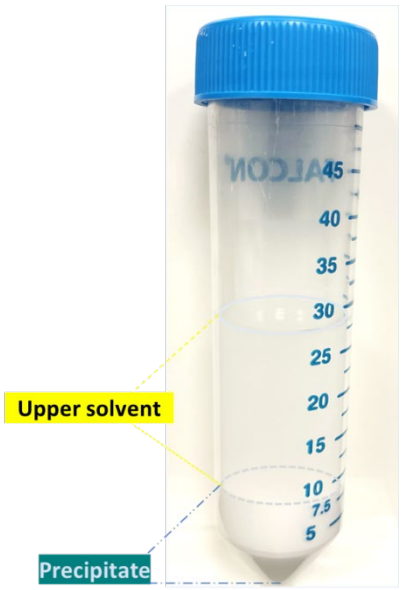

Figure S2. Phase separation after $CaCl_2$ was added.

S.3. SEM images of $CaCO_3$ of different magnifications and samples

The particles in **Fig. S2** were observed using SEM after washing and centrifugation. The SEM images (**Fig. S3**) were used for size distribution estimation.

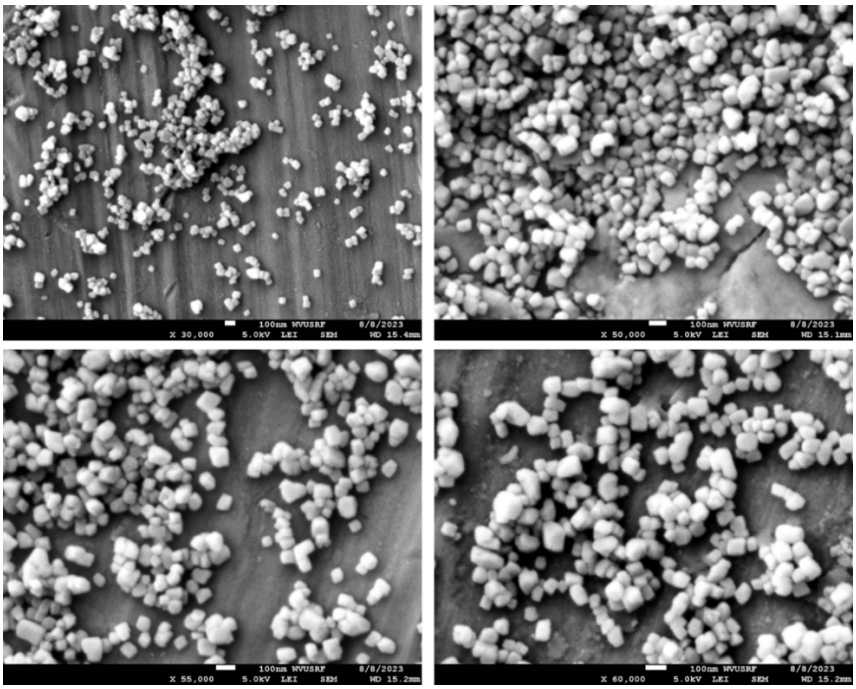

Figure S3. SEM images of different magnifications and samples.

S.4. SEM images of $CaCO_3$ produced by different amino acid with the dosage of 0.025 mol

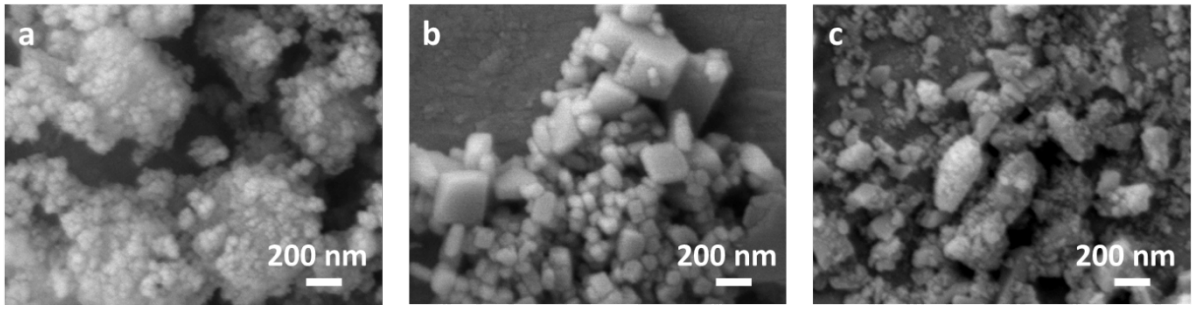

Figure S4. $CaCO_3$ prepared from a) Asn, b) Ala, and c) Cys with the dosage of 0.025 mol. Experimental conditions: Asn (0.025 mol), Ala (0.025 mol), Cys (0.025 mol), NaOH (0.05 mol), $CaCl_2$ (0.05 mol), CO_2 gas flow rate (100 sccm), and CO_2 bubbling time (20 min).

S.5. CO_2 loading $CaCO_3$ conversion based upon Gly concentration

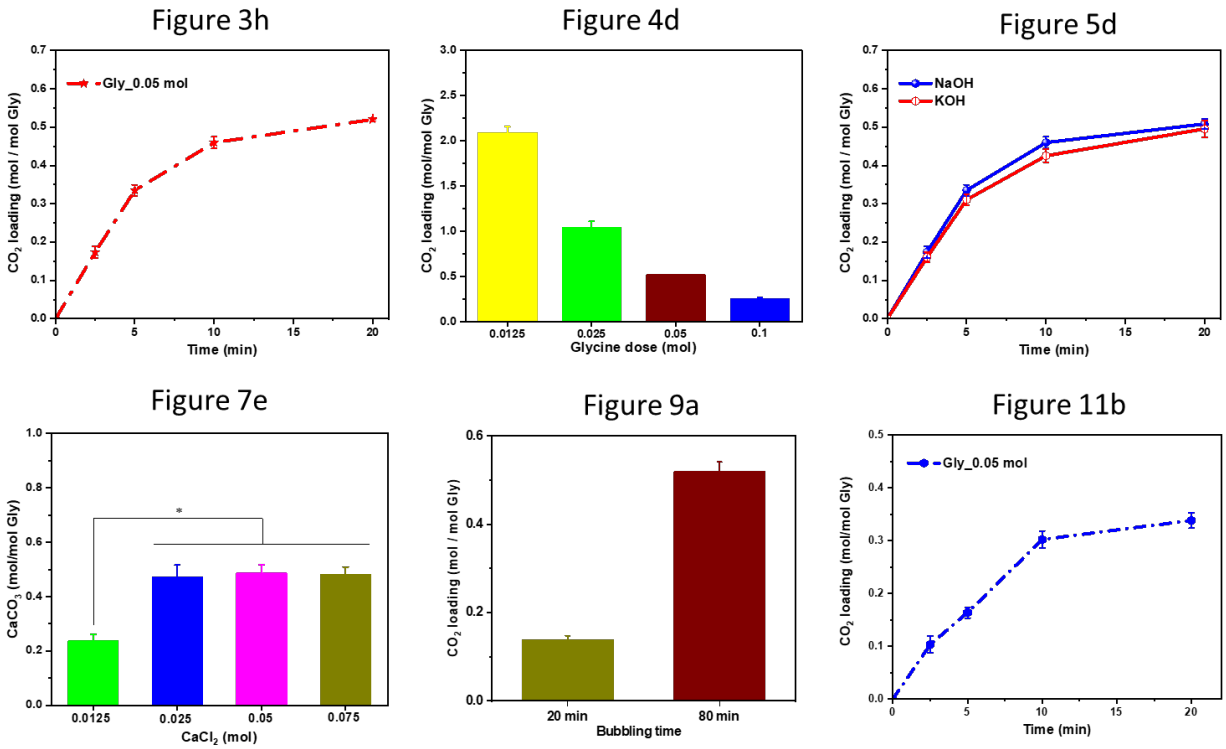

Reference

[1] Z. Bao, Q. Li, N.G. Akhmedov, B.A. Li, M. Xing, J. Wang, B.I. Morsi, B. Li, Innovative cycling reaction mechanisms of CO_2 absorption in amino acid salt solvents, Chem. Eng. J. Adv. (2022) 100250. https://doi.org/https://doi.org/10.1016/j.ceja.2022.100250.

[2] Q. Li, Z. Bao, N.G. Akhmedov, B.A. Li, Y. Duan, M. Xing, J. Wang, B.I. Morsi, B. Li, Unraveling the Role of Glycine in K_2CO_3 Solvent for CO_2 Removal, Ind. Eng. Chem. Res. 61(34) (2022) 12545-12554. https://doi.org/https://doi.org/10.1021/acs.iecr.2c01637.

[3] X. Wang, N.G. Akhmedov, D. Hopkinson, J. Hoffman, Y. Duan, A. Egbebi, K. Resnik, B. Li, Phase change amino acid salt separates into CO_2-rich and CO_2-lean phases upon interacting with CO_2, *Appl. Energy* 161 (2016) 41-47. https://doi.org/10.1016/j.apenergy.2015.09.094.